A one-dimensional stochastic model of turbulence within and above plant canopies

Livia S. Freire[a], Marcelo Chamecki[b,*]

[a] *Department of Meteorology, Pennsylvania State University, University Park PA, 16802, USA*
[b] *Department of Atmospheric and Oceanic Sciences, University of California, Los Angeles, Los Angeles, CA 90095, USA*

Abstract

The suitability of Kerstein's One-Dimensional Turbulence (ODT) model in the representation of atmospheric boundary layer (ABL) flows within and above plant canopies is investigated. The ODT model was adapted to represent a filtered version of flow and scalar fields, equipped with a Smagorinsky-like sub-grid scale model, a wall model, and a parameterization of the canopy effects on the flow. In the filtered ODT, the entire vertical extension of the ABL is modeled and the "resolved" vertical turbulent transport is represented by stochastic eddies that effectively mix fluid parcels across a path length, representing non-local turbulent fluxes that are a critical feature of the canopy roughness sublayer. Simulations for different canopies and stability conditions are performed and vertical profiles of turbulence and scalar statistics are compared with observational and large-eddy simulation data. This new filtered version of the ODT model yields grid-independent results. Model performance for plant canopies is consistent with previous results from ODT for all cases tested without any case-specific parameter adjustment, generating reasonable agreement in profiles of mean velocity, temperature and water vapor mixing ratio, as well as vertical fluxes of momentum and sensible and latent heat, despite the underestimation of all velocity variances. Non-local transport is intrinsic to the formulation of ODT, which represents a significant advantage compared to other reduced-model approaches employed for canopy flows.

Keywords: canopy turbulence, one dimensional model, column model, non-local flux

1. Introduction

The dynamic interaction between plant canopies and the flow in the atmospheric boundary layer (ABL) leads to the formation of a turbulent flow with attributes that significantly differ from those characteristic of classical surface-layer turbulence. The drastic reduction in streamwise velocity inside the canopy due to drag produces an inflection in the mean velocity profile, leading to the production of coherent eddies via shear instability that scale with the canopy height. The action of these large eddies on mean profiles of momentum and scalars that display large changes across vertical distances comparable to the canopy height lead to non-local turbulent fluxes that dominate the transport in the canopy region (Finnigan, 2000). Such complex turbulent flow presents a challenge for the development of simple numerical models.

Most of the interest in modeling canopy flows is motivated by the need of robust approaches to quantify land-atmosphere exchanges of momentum, energy, gases, and particles. These exchanges are needed, for example, when computing energy and carbon budgets (Juang et al., 2008), chemical reactions in forest environments (Bryan et al., 2012), and pollen and spores emission rates and dispersion (Pan et al., 2014). In air-quality, weather and climate models, the parameterization of land-atmosphere exchanges depends on the appropriate representation of flow inside the canopy. In the simplest cases, a vertical profile of the mean wind velocity and scalar concentration within and above the canopy can be obtained by empirical models based on similarity theory and dimensional analysis, such as the ones presented by Yamazaki et al. (1992), Harman and Finnigan (2007) and Harman and Finnigan (2008). To represent more complex interactions, vertical profiles of higher-order turbulence statistics (such as variances and fluxes) are needed, and in this case the most common approach is to use Reynolds-averaged Navier-Stokes (RANS) equations for the flow field and Reynolds-averaged conservation equations for temperature and any other scalars of interest. Under steady-state and horizontally-homogeneous conditions, the equations can be reduced to a set of coupled ODEs for the mean fields and for variances and vertical fluxes of momentum and scalars. Invoking a second-order closure scheme yields a set of equations that can be solved numerically or analytically, depending on the assumptions adopted (Wilson and Shaw, 1977; Massman and Weil, 1999). This approach has a low computational cost and can provide useful results given the appropriate closure and calibration (Katul and Albertson, 1998; Massman and Weil, 1999). However, the number of equations to be resolved and the number of closure assumptions and parameters to be adjusted increases fast if the transport of many scalar fields (e.g. temperature, water vapor, carbon dioxide, etc.) are to be included (Juang et al., 2008). For the case of transport of scalars inside canopies, an alternative solution is obtained using a Lagrangian stochastic methodology based on the Langevin equation (e.g., see Thomson, 1987; Wilson and Sawford, 1996). However, this modeling approach is incomplete, as it requires specification of the vertical profiles of turbulence statistics. These profiles are

*Corresponding author. E-mail address: chamecki@ucla.edu

typically obtained from experiments (e.g. Reynolds, 1998; Cassiani et al., 2007) or from RANS models described above (e.g. Katul et al., 2011; Gleicher et al., 2014).

On the other end of the spectrum is Large-Eddy Simulation (LES). Together with field and wind-tunnel experimental data, LES results have been fundamental to the advancement of knowledge of three-dimensional turbulence and dispersion in the canopy environment. However, due to the high computational cost, most LES of canopy flows have domain sizes too small to represent the entire ABL (as found in Dwyer et al. (1997); Su et al. (1998); Albertson et al. (2001); Huang et al. (2013); Pan et al. (2014)), and only very recently a simulation resolving the canopy flow and the entire ABL simultaneously has been performed (Patton et al., 2016). With the increasing demand for inclusion of complex processes (such as chemical reactions and particle dispersion) combined with the use of large domains and higher resolutions close to the surface, the technique is currently limited by the computational power available, creating an opportunity for the development of alternative modeling approaches.

In this work we investigated the suitability of Kerstein's One-Dimensional Turbulence (ODT) model (Kerstein, 1999) in the representation of canopy turbulence in the ABL. In the context of ABL simulations, ODT can be viewed as a single-column model with a stochastic representation of turbulent transport. In the ODT framework, unsteady, one-dimensional diffusion equations for momentum, temperature and passive scalars are solved numerically on a discrete grid, and the turbulent transport is represented by stochastic eddy events. As a modeling tool for canopy flows under horizontally-homogeneous conditions, ODT has the potential to be an intermediate approach between RANS and LES in terms of computational cost and model applicability. When compared to LES, the main advantage of ODT is the much lower computational cost, allowing the simulation of larger vertical domains with better resolutions in the canopy region, as well as its applicability as a sub-model in complex geophysical numerical models. When compared to simpler single column models, ODT has many advantages: (i) it is not based on eddy-diffusivity closures and it explicitly represents non-local turbulence fluxes through non-local stochastic eddies already present in its original formulation; (ii) it can represent multiple scalar fields (including coupled source/sink and concentration profiles) in a straight-forward way without increasing the number of closure assumptions and adjustable parameters; and (iii) it allows for the possibility of simulating transient (non-equilibrium) conditions or converting the time dimension into streamwise dimension, allowing the representation of two-dimensional steady-state flows (useful for plume-growth studies, for example). The main limitation is that results can only be evaluated in terms of ensemble averages due to the stochastic nature of the turbulence in the model.

The ODT model studied here was first developed with a single velocity component and temperature fields by Kerstein (1999), and further extended to represent a three-component velocity vector plus the temperature field by Kerstein et al. (2001). ODT was shown to reproduce important characteristics of several canonical turbulent flows including homogeneous turbulence, shear layers, buoyancy-driven flows (Kerstein, 1999), mixing-layer and wakes (Kerstein et al., 2001). Overall, ODT provided results comparable do Direct Numerical Simulation (DNS) for the profiles of mean velocity, temperature and passive scalar concentration, as well as profiles of momentum flux, whereas profiles of velocity variances showed significant underprediction. ODT also reproduces the correct inertial-range spectral behavior in both homogeneous decaying and stationary turbulence, in addition to the correct cascade in the density spectrum of a buoyancy-driven flow (Kerstein, 1999), showing the ability of the stochastic representation of turbulence in mimicking important three-dimension features of a true turbulent flow. A smooth channel simulation with friction Reynolds number $Re_\tau = u_* H/\nu = 590$ (where u_* is the friction velocity, H is half of the channel width and ν is the kinematic viscosity) also generated profiles of mean velocity and momentum flux very close to DNS results, but velocity variances were underestimated for all three components (Schmidt et al., 2003). In all these cases, two model parameters, one relating the occurrence of stochastic eddies with the amount of energy available and another defining the timescale of viscous cutoff, had to be adjusted.

Simulations of a stably stratified ABL using ODT were presented by Kerstein and Wunsch (2006), where for the first time the model was used in a "large-eddy simulation mode" in order to keep the computational cost low. In this case, the model resolution did not resolve the Kolmogorov dissipative scales, and a subgrid-scale (SGS) viscosity was invoked. Two approaches were tested for the SGS model, one with fixed eddy viscosity values and another with a variable eddy viscosity that depended on the local resolved flow properties. Results showed the consistent ODT behavior of correct profiles of mean velocity and potential temperature, as well as profiles of momentum and heat fluxes, but with underestimation of variances. Neither SGS closure proposed was considered satisfactory, given that they required the adjustment of a new parameter that was not independent on grid resolution, leading the authors to the conclusion that a better SGS closure is needed in order to yield a cost-effective ABL simulation tool. To this end, a one-dimensional adaptation of the classic Smagorinsky eddy viscosity model (Smagorinsky, 1963) used in LES (Deardorff, 1970) is developed and tested here.

Section 2 presents a description of the ODT model, including the new SGS model and the modifications introduced to represent the canopy. A brief description of the experimental and LES data sets used for comparison and the model setup are given in Section 3. Simulation results for a smooth channel flow with $Re_\tau = 5200$, a maize canopy and a model of waving wheat crop under neutral conditions, and a deciduous case under neutral, unstable and free-convection conditions are presented in Section 4. Conclusions and potential uses for the ODT model are discussed in Section 5.

2. Model description

2.1. Kerstein's One-Dimensional Turbulence model

In this subsection a short but complete description of the ODT model is presented. For a more detailed discussion of the modeling approach, the reader is referred to Kerstein (1999) and Kerstein et al. (2001).

The ODT model represents the time evolution of the velocity vector, temperature and additional scalar fields along a line. One-dimensional unsteady diffusion equations are discretized and solved numerically while the effect of turbulence is modeled by instantaneous stochastic eddy events. In the present work, the ODT domain corresponds to a vertical line representing the time evolution of a horizontally homogeneous ABL column with zero mean vertical velocity (i.e., there is no mean advection). The continuity equation is not included in the model due to its one-dimensional nature, and the governing equations can be written as (Kerstein and Wunsch, 2006):

$$\frac{\partial u_i}{\partial t} = F_i + f\,(u_2\delta_{i1} - u_1\delta_{i2}) + \nu\frac{\partial^2 u_i}{\partial x_3^2} + \textbf{eddy events}, \tag{1}$$

$$\frac{\partial \theta}{\partial t} = Q_\theta + \frac{\nu}{Pr}\frac{\partial^2 \theta}{\partial x_3^2} + \textbf{eddy events}, \tag{2}$$

where x_i is the vector representing the three spatial directions (x_3 is the vertical direction), t is time, $u_i(x_3, t)$ is the velocity vector, $\theta(x_3, t)$ is the potential temperature, F_i is a constant mean pressure gradient force that drives the flow, f is the Coriolis parameter, Q_θ is a heat source/sink, ν is the kinematic viscosity, Pr is the Prandtl number, and δ_{ij} is the Kronecker delta. For simulations where the Coriolis force is not present (such as the smooth channel flow presented here), the flow is driven by a constant, streamwise mean pressure gradient force F_1 ($F_2 = F_3 = 0$). When the Coriolis force is present, geostrophic balance is assumed above the ABL and the mean pressure gradient force is written as $F_i = f\left(U_g\delta_{i2} - V_g\delta_{i1}\right)$, where (U_g, V_g) is a constant horizontal geostrophic wind.

The time evolution of any additional passive scalar can be represented in the model by an additional equation similar to Equation (2), if all physical and chemical sources/sinks are represented by Q_{scalar} and after replacing the Prandtl number Pr by the appropriate Schmidt number Sc.

The instantaneous eddy events in Equations (1) and (2) consist of two mathematical operations representing the effects of advection, gravitational potential energy and pressure fluctuations (Kerstein and Wunsch, 2006). In practice, when an eddy event is selected, the variables at the position z (hereafter z corresponds to the vertical direction x_3) are instantaneously replaced by the values at $M(z)$ (a mapping function) in the following way:

$$u_i(z) \rightarrow u_i(M(z)) + c_i K(z), \tag{3}$$

$$\theta(z) \rightarrow \theta(M(z)). \tag{4}$$

The first term on the right-hand side of Equations (3) and (4) is a model for advection by a turbulent eddy based on a triplet map. The mapping function is chosen so that it is conservative (i.e., it preserves the total amount of the quantity being transported) and does not introduce discontinuities. In addition, it mimics the energy cascade in turbulence by transferring energy from large to small scales in a scale-local fashion (via stretching-folding approach). Defining z_b as the position of the bottom of the eddy and l as its vertical size, the triplet map can be mathematically expressed as (Kerstein et al., 2001)

$$M(z) = z_b + \begin{cases} 3(z - z_b), & \text{if } z_b \le z \le (z_b + l/3), \\ 2l - 3(z - z_b), & \text{if } (z_b + l/3) \le z \le (z_b + 2l/3), \\ 3(z - z_b) - 2l, & \text{if } (z_b + 2l/3) \le z \le (z_b + l), \\ z - z_b, & \text{otherwise.} \end{cases} \tag{5}$$

As described by Kerstein and Wunsch (2006), the triplet map "takes a line segment, shrinks it to a third of its original length, and then places three copies on the original domain. The middle copy is reversed, which maintains continuity of advected fields and introduces the rotational folding effect of turbulent eddy motion."

The second term on the right-hand size of Equation (3) is a kernel function that acts on the kinetic energy of the flow. It increases/reduces the total kinetic energy of the region within the eddy based on the local temperature profile (through a potential energy quantification based on the Boussinesq approximation) and it redistributes the final energy among the three velocity components, mimicking a pressure-induced tendency towards isotropy on the flow. In this term, $K(z) = z - M(z)$ is the distance that the fluid parcel is displaced during an eddy event, and c_i corresponds to the amplitude of energy redistribution.

The variation of kinetic energy ΔE_i and potential energy ΔE_g (per unit mass) during an eddy event can be written as

$$\Delta E_i = \frac{1}{2l}\int_{z_b}^{z_b+l} [(u_i(M(z)) + c_i K(z))^2 - u_i^2(z)]dz, \tag{6}$$

$$\Delta E_g = -\frac{g}{l}\int_{z_b}^{z_b+l} \frac{[\theta(M(z)) - \theta(z)]}{\theta_0} z dz, \tag{7}$$

where g is the gravitational acceleration and θ_0 is a reference temperature. The coefficients c_i in Equation (3) are determined by requiring total energy conservation, i.e. $\sum_i \Delta E_i + \Delta E_g = 0$, which gives

$$\sum_i \left[l\, c_i\, u_{K,i} + \frac{2}{27} l^2 c_i^2 \right] - g l \frac{\theta_K}{\theta_0} = 0, \tag{8}$$

where the equality $\int_{z_b}^{z_b+l} K^2(z)dz = 4l^3/27$ was used, in addition to the fact that the result of any integral over $M(z)$ is equal to the integral of the same function over z. Also, the new variable

$$n_K \equiv \frac{1}{l^2}\int_{z_b}^{z_b+l} n(M(z))K(z)dz \tag{9}$$

was defined for $n = u_i$ or θ.

In addition to Equation (8), two extra conditions are needed to close the system and determine values of c_i. The first is a definition of the maximum amount of energy that can be extracted

from one velocity component during the eddy event, which is obtained from a maximization of -ΔE_i with respect to c_i, resulting in an amount of $27\,l\,u_{K,i}^2/8$. The second condition determines the tendency towards isotropy of the model, by forcing the total available energy to be equally distributed among the velocity components (see Kerstein et al. (2001) for details and a discussion on these final constrains). The final equation for c_i can be written as

$$c_i = \frac{27}{4l}\left[-u_{K,i} \pm \sqrt{\frac{1}{3}\left(u_{K,1}^2 + u_{K,2}^2 + u_{K,3}^2 + \frac{8gl}{27}\frac{\theta_K}{\theta_0}\right)}\right], \quad (10)$$

where the quantity inside the parenthesis represents the total amount of energy available for redistribution, and the sign ambiguity corresponds to the sign of $u_{K,i}$.

Equations (3), (4), (5) and (10) describe the effect of the occurrence of an eddy event on the velocity and temperature profiles. Another key feature that determines the success of the model is the choice of the sequence of eddy events that occur during a simulation. The probability distribution that governs the occurrence of stochastic eddies in ODT is linked to the instantaneous velocity and temperature fields being simulated. At a given time t, λ is defined as the probability of occurrence of eddies with a size l at the location z_b. From dimensional arguments, λ is proportional to $(l^2\tau)^{-1}$, where $\tau(z_b, l, t)$ is the eddy turnover time scale,

$$\lambda(z_b, l, t) \equiv \frac{C_\lambda}{l^2\tau(z_b, l, t)}, \quad (11)$$

and C_λ is a constant of proportionality. Furthermore, the time scale $\tau(z_b, l, t)$ can be related to the total amount of energy available by dimensional arguments via

$$\frac{l^2}{\tau^2} \sim u_{K,1}^2 + u_{K,2}^2 + u_{K,3}^2 + \frac{8gl}{27}\frac{\theta_K}{\theta_0} - \frac{Z_\lambda \nu^2}{l^2}. \quad (12)$$

For simulations resolving the Kolmogorov scales, the last term of Equation (12) represents the damping effect of viscosity, because any eddy with a time scale much longer than the viscous time scale should be prohibited (Z_λ is an adjustable parameter). For simulations that do not resolve the Kolmogorov scales, $Z_\lambda = 0$. The final form of the distribution λ is

$$\lambda(z_b, l, t) = \frac{C_\lambda}{l^3}\sqrt{\frac{1}{3}\left(u_{K,1}^2 + u_{K,2}^2 + u_{K,3}^2 + \frac{8gl}{27}\frac{\theta_K}{\theta_0}\right) - \frac{Z_\lambda \nu^2}{l^2}}, \quad (13)$$

where the $1/3$ in front of the available energy is kept for consistency with the results presented by Schmidt et al. (2003), which will be used as a starting point for the present study. Note that the $1/3$ factor is sometimes included in the definition of the constants C_λ and Z_λ (as in Kerstein and Wunsch (2006), for example). The value of C_λ in Equation (13) is used to regulate the number of eddies allowed for a given energy availability in the flow, effectively setting the turbulent intensity. Finally, this formulation gives the correct critical Richardson number of 1/4 for the suppression of eddy events by stable stratification (Kerstein and Wunsch, 2006).

Some important characteristics of ODT deserve clarification. First, due to the one-dimensional nature of the model, continuity cannot be invoked and the three velocity components remain uncorrelated throughout the simulation. In other words, each velocity component evolves in time as an independent scalar field. If all velocity components are subject to the same forcing, initial and boundary conditions, their statistics remain identical. Furthermore, the velocity components do not collectively represent a physical evolving flow feature such as a three-dimensional turbulence structure, and although the stochastic eddies mimic the effect of a three-dimensional turbulent eddy, the velocity components are not associated with a specific eddy event. Consequently, even though the velocity vector defines the probability distribution of eddy events, vertical velocity fluctuations are not directly responsible for vertical advection. Instead, vertical advection is caused by each eddy event (i.e. the instantaneous shuffling produced by the triplet map). Thus, the role of the velocity vector in the simulation is to convert the information about the body forces and boundary conditions into a time evolving probability distribution of eddy events whose accumulated effect resembles that of the real turbulent flow.

The kinetic energy associated with each velocity component can originate from two sources: imposed forces acting along that direction and pressure redistribution. In the ABL simulations presented here, both horizontal components are subject to external forcing via mean pressure gradient and Coriolis. Thus, both u_1 and u_2 are impacted by shear production of turbulent kinetic energy (TKE). However, it is important to point out that because buoyancy effects are introduced in the stochastic eddy formulation without actually accelerating the flow in the vertical direction, the only source of vertical velocity variance is the pressure redistribution effect, making vertical velocity statistics less realistic than those for the other two velocity components. Nevertheless, the vertical velocity component still carries part of the TKE of the flow and should therefore be taken into account as part of the velocity field (it should enter the subgrid-scale model formulation, for example).

A consequence of the way velocity impacts the evolution of the simulation in ODT is the possibility of using only one velocity component when simulating flows in which TKE is produced in only one direction, as was done by Kerstein (1999). In this case, this single velocity drives the probability distribution from which the eddy events are selected, creating all the turbulence of the flow. The main motivation for introducing the vector formulation is the possibility of implementing an energy transfer among velocity components, mimicking the tendency towards isotropy on the flow (one of the consequences of continuity) and increasing the reality of the simulation (Kerstein et al., 2001). Furthermore, having the three velocity components enables the representation of flows with forcing in more than one direction, as it is the case of Coriolis and drag forces in the ABL, for example. In addition, the velocity vector representation facilitates the coupling of ODT to other three-dimensional models.

Another consequence of ODT formulation is the fact that all vertical turbulent transport is caused by the eddy events, rather than by the fluctuating vertical velocity directly. Therefore, the

vertical turbulent fluxes are estimated from the accumulated transport caused by a series of stochastic eddy events. For a time interval Δt, the mean vertical turbulent flux of any quantity n ($n = u_i$ or θ) is obtained from the sum of changes on its value due to stochastic eddies, calculated as

$$\text{eddy flux}_n(z) = \frac{1}{\Delta t}\int_z^H \sum_{\text{t}}^{t+\Delta t}[n_{\text{after}}(z') - n_{\text{before}}(z')]dz' \qquad (14)$$

where H is the height of the domain and $n_{\text{before}}(z)$ and $n_{\text{after}}(z)$ correspond to the values of n at given position z before and after the occurrence of an eddy event. Note that, because of this ODT characteristic, the vertical flux of a variable n, which is commonly represented by $\overline{u_3' n'}$, will be denoted here by the term "eddy flux$_n$". A consequence of this decoupling between vertical velocity fluctuations and vertical transport is that correct flux predictions can be obtained even if the vertical velocity variance is not correct.

Equations (1) to (14) represent the basis of the ODT model, which has been used to reproduce multiple types of turbulent flows (Kerstein, 1999; Kerstein et al., 2001). In summary, the simulation evolves in time with Equations (1) and (2), and in each time step the current velocity and temperature profiles determine the probability distribution of eddies λ (Equation (13)). This distribution is used to randomly select eddies that act instantaneously on the velocity and temperature fields through Equations (3), (4), (5) and (10), after which the simulation advances to the next time step. Next subsections describe the new subgrid-scale parameterization and the modifications required to represent the canopy drag in the ODT.

2.2. Subgrid-scale and wall models

In most of the previous applications, the ODT model has been used to represent turbulent flows down to the Kolmogorov scale (e.g. Kerstein, 1999; Schmidt et al., 2009). However, in channel flow simulations that resolve the viscous layer (using approximately 15 grid points) the computational cost of ODT simulations increases at a rate proportional to approximately Re_τ^2 (based on numerical tests with $325 \leq Re_\tau \leq 5200$). This large increase is, in part, caused by the required reduction in time step with increasing Reynolds number. Thus, while the simulation for $Re_\tau = 5200$ runs in one or two hours on a personal computer, a simulation for the entire ABL with $Re_\tau \sim 10^7$ would have a prohibitive computational cost. Furthermore, the relevance of molecular transport in the ABL is restricted to the near-surface region, whose rough nature requires a bulk parameterization anyway. Therefore, following the common practice in LES, we introduce a filter to formally separate resolved and sub-grid scales. In this filtered ODT model, resolved scales can be defined by filtering the velocity and temperature fields at the scale $\Delta = dz$. Equations (1) and (2) become

$$\frac{\partial \tilde{u}_i}{\partial t} = F_i + f\,(\tilde{u}_2\delta_{i1} - \tilde{u}_1\delta_{i2}) - \frac{\partial \tau_{i3}}{\partial x_3} + \textbf{eddy events}, \qquad (15)$$

$$\frac{\partial \tilde{\theta}}{\partial t} = Q_\theta - \frac{\partial \chi_3}{\partial x_3} + \textbf{eddy events}, \qquad (16)$$

where $\tilde{u}_i$ and $\tilde{\theta}$ are the resolved velocity and temperature fields, τ_{i3} is the SGS vertical stress vector and χ_3 is the SGS vertical heat flux. The molecular/viscous terms are removed as they are negligible at the Reynolds numbers of the atmosphere. In the present approach the numerical grid dictates the smallest resolved eddy size and thus effectively sets the scale Δ, as typically done in most LES models.

The SGS terms τ_{i3} and χ_3 are modeled using a one-dimensional analogy to the eddy-viscosity model

$$\tau_{i3} = -\nu_{\text{SGS}}\frac{\partial \tilde{u}_i}{\partial x_3}, \qquad (17)$$

$$\chi_3 = -\frac{\nu_{\text{SGS}}}{Pr_{\text{SGS}}}\frac{\partial \tilde{\theta}}{\partial x_3}, \qquad (18)$$

where Pr_{SGS} is the SGS Prandtl number (a constant value $Pr_{\text{SGS}} = 0.4$ is adopted in all simulations) and ν_{SGS} is the SGS eddy-viscosity represented using a one-dimensional version of the Smagorinsky model (Smagorinsky, 1963)

$$\nu_{\text{SGS}} = (C_s\Delta)^2\left[\frac{\partial \tilde{u}_i}{\partial z}\frac{\partial \tilde{u}_i}{\partial z}\right]^{1/2}, \qquad (19)$$

where C_s is the Smagorinsky coefficient. A minimum value of 1.5×10^{-5} m^{2}s^{-1} is imposed for ν_{SGS}, a necessary condition for situations where velocity gradients are zero (such as in the inversion layer above the ABL). For three-dimensional homogeneous isotropic turbulence, Lilly (1967) obtained $C_s \approx 0.17$ as the optimal value for simulations where the filter cutoff was in the inertial subrange. For channel flows, Deardorff (1970) and Piomelli et al. (1988) used $C_s = 0.1$. In true Navier-Stokes turbulence it is known that this value should be smaller for regions of high shear such as near a wall (Deardorff, 1970), and that significant model performance can be accomplished by using dynamically determined coefficients (Germano et al., 1991; Porté-Agel et al., 2000). In this study, the wall-damping function proposed by Mason and Thomson (1992) of the form

$$\frac{1}{(C_s\Delta)} = \frac{1}{(C_{s,0}\Delta)} + \frac{1}{\kappa(z+z_0)} \qquad (20)$$

is used, with $C_{s,0} = 0.1$ and $\Delta = dz$ (z_0 is the roughness length). Dynamically evaluated coefficients following the approaches of Germano et al. (1991) and Porté-Agel et al. (2000) were also implemented, but they did not improve significantly the results in ODT simulations.

For ABL simulations over rough surfaces, the no-slip boundary condition for the horizontal velocities cannot be enforced directly, and a wall model is needed. For simplicity, the equilibrium wall-model used in LES of ABL flows is also used here. The specific implementation employed here uses the Monin-Obukhov similarity functions to determine the wall stress as a function of the resolved velocity at the first grid point following the approach described in Kumar et al. (2006):

$$\tau_w = -\left[\frac{\kappa}{\ln(dz/z_0)} - \psi_M\right]^2[\tilde{u}_1^2(dz) + \tilde{u}_2^2(dz)], \qquad (21)$$

$$\tau_{i3}^{wall} = \tau_w\left\{\frac{\tilde{u}_i(dz)}{[\tilde{u}_1^2(dz) + \tilde{u}_2^2(dz)]^{1/2}}\right\}, \qquad (22)$$

where τ_w is the total wall shear stress, τ_{i3}^{wall} is the partitioning of the total shear stress into x_1 and x_2 directions, $\tilde{u}_i(dz)$ are the horizontal velocities at the first grid point, and ψ_M is defined in terms of the Monin-Obukhov similarity function for the mean velocity gradient as $\psi_M = \int_{z_0/L}^{z/L}(1 - \phi_M(x))x^{-1}dx$. The same set of similarity functions adopted by Kumar et al. (2006) is employed here.

2.3. Canopy parameterization

Air flow through the vegetation is subjected to interactions with the vegetation elements (leaves, branches, etc.), which result in viscous and pressure drag forces on the flow. The pressure drag is the dominant component and the viscous drag is neglected here (as usually done in LES – Shaw and Schumann (1992); Pan et al. (2014); Patton et al. (2016)). Distinct models are employed to represent the effect of pressure drag on the resolved flow and on the stochastic eddies. The former is done through the inclusion of a body force d_i on the right-hand side of Equation (15). Following the usual approach in LES, the force is proportional to the leaf area density $a(z)$ and the square of the local velocity, with the constant of proportionality being the drag coefficient C_d, resulting in

$$d_i = -C_d a P_{ij}\tilde{u}_j(\tilde{u}_k\tilde{u}_k)^{1/2}. \tag{23}$$

Here, P_{ij} is the projection matrix, included to create an effective partition of the leaf area density facing the three spatial directions (Pan et al., 2014).

To model the effects of pressure drag on the stochastic eddies, we use a simple parameterization based on the approach developed by Shaw and Patton (2003) to represent the loss of subgrid scale energy to pressure drag. Eddy events that penetrate into the canopy region no longer conserve total energy and the energy loss is given by the total work against pressure drag, modeled as

$$E_d = \frac{8}{3}C_d P \int_{z_b}^{z_b+l} a(z)e(z)dz, \tag{24}$$

where $P = P_{ii}/3$ and $e = (\tilde{u}_1^2 + \tilde{u}_2^2 + \tilde{u}_3^2)/2$ is the resolved kinetic energy. Equation (24) assumes isotropic and non-skewed kinetic energy (Shaw and Patton, 2003), assumptions that are used here for simplicity. Note that by using the average drag over the entire eddy instead of a purely local drag effect, the flow within the entire eddy will be impacted by the canopy, even if only part of the eddy penetrated into the canopy region.

In terms of the ODT modeling framework, now the energy equation is replaced by $\sum_i \Delta E_i + \Delta E_g = E_d$, which in practice results in a new equation for c_i that replaces Equation (10)

$$c_i = \frac{27}{4l}\left\{ - u_{K,i} \pm \sqrt{\frac{1}{3}\left[u_{K,1}^2 + u_{K,2}^2 + u_{K,3}^2 + \frac{8}{27}\left(gl\frac{\theta_K}{\theta_0} - \frac{8}{3}C_d P\int_{z_b}^{z_b+l} a(z)e(z)dz\right)\right]}\right\}. \tag{25}$$

Equations (12) and (13) are not modified, so the energy loss given by (24) does not impact directly the probability of occurrence of eddies. Once an eddy event is chosen, if that eddy penetrates into the canopy region it looses energy to the drag force exerted by the canopy.

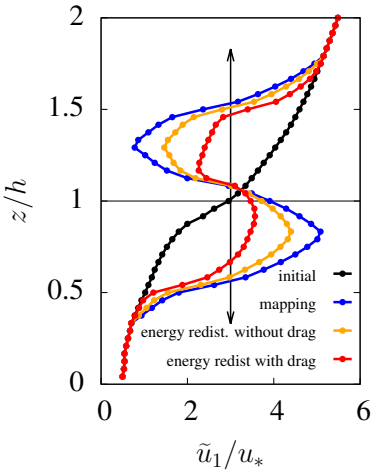

Figure 1: Example of the effect of a stochastic eddy on the streamwise velocity profile. Illustrative case assuming initial profile of $\tilde{u}_1$ (black) equal to the mean streamwise velocity in a maize canopy, and $\tilde{u}_2 = \tilde{u}_3 = 0$. Profile after mapping function (blue), and after the energy redistribution without (orange) and with (red) loss of energy to canopy drag. Vertical arrow indicates the size and location of the stochastic eddy.

Figure 1 illustrates the impact of a stochastic eddy that scales with canopy height in the streamwise velocity profile. For illustration purposes the mean velocity profile was used (i.e. $\tilde{u}_1 = \overline{u}_1$ and $\tilde{u}_2 = \tilde{u}_3 = 0$), even though stochastic eddies act on the instantaneous profiles that deviate from the mean state during the simulation. First, as described in subsection 2.1, the mapping function (Equation (5)) causes mixing and vertical transport without changing the total momentum inside the eddy and without creating discontinuities on the profile (blue curve). Subsequently, the kernel function redistributes the total energy among the three velocity components, which in this example reduced the streamwise velocity by transferring energy to the other two components (yellow curve). In the newly implemented canopy formulation, an additional loss of energy due to canopy drag is introduced, reducing the total amount of energy available for redistribution and consequently the final amount of momentum in streamwise direction (red curve). The final streamwise velocity profile is significantly different from the original one, incorporating the effects of non-local turbulent transport and canopy drag.

3. Simulations setup, observational and Large-Eddy Simulation data

3.1. Smooth channel flow

As a first test of the filtered ODT with the new SGS and wall models, simulations of a smooth channel flow with $Re_\tau = u_* H/\nu = 5200$ were performed and compared with DNS results obtained by Lee and Moser (2015). For comparison, results were obtained from a simulation with the ODT version presented by Schmidt et al. (2003), in which ODT was used in

"DNS mode", i.e., resolving all scales down to the Kolmogorov scales (Equations (1) and (2)). The domain corresponded to $2H$, the number of grid points was set to 10400 and the flow was driven by a constant streamwise mean pressure gradient force $F_1 H/u_*^2 = 1$. No-slip boundary conditions ($u_i = 0$) were imposed on both ends of the domain. The values of $C_\lambda = 12.73$ and $Z_\lambda = 98$ selected by Schmidt et al. (2003) were used. No temperature or scalar fields were included. Initial conditions were zero velocity vector plus small ($\sim 10^{-8}$) random fluctuations, and the simulation ran for 1000 seconds. Results presented here correspond to an average over the last 990 seconds. No ensemble average was performed, as the large averaging period was sufficient to ensure statistical convergence.

The comparison of ODT results in "LES mode" (i.e., not resolving the Kolmogorov scales and including the SGS and wall models) with this reference ODT simulation in "DNS mode" was performed with a simulation using the same domain and pressure gradient force, but with 200 grid points. Because the lowest grid point was in the inertial region of the flow where the log-law is valid, the wall model described in Section 2 was invoked as boundary conditions in the horizontal directions (the value of $z_0/H = 2.4 \times 10^{-5}$, equivalent to the law-of-the-wall $\overline{u}_1/u_* = (1/\kappa)\ln(zu_*/\nu) + 5.1$, was adopted). The boundary condition for the vertical velocity was $\tilde{u}_3 = 0$ at both walls. The value of Z_λ was set to zero as the viscous scales were not resolved, and all the other simulation parameters (including the adjustable parameter C_λ) were set to the same values of the ODT simulation in "DNS mode". Three additional simulations of ODT in "LES mode" with different number of grid points (100, 400 and 600) were performed to evaluate possible grid-dependence of the SGS model.

3.2. Maize canopy

The first set of canopy simulations were designed to match the Mahomet maize canopy experiment described by Gleicher et al. (2014). Here, we used as a reference the profiles of mean flow and turbulence statistics from a 2.1 m tall maize canopy, obtained during near-neutral atmospheric stability conditions in the period between 9:30 and 17:00 local time (broken into fifteen 30-min runs) on 10 July 2011.

Two distinct simulations of the maize canopy were performed. The first is similar to the LES performed by Pan et al. (2014), where the domain corresponded to a a 42 m-tall half-channel flow, driven by a constant mean streamwise pressure gradient force $F_1 = 5 \times 10^{-3}\,\mathrm{m\,s^{-2}}$. A total of 480 grid points were used (twice the number used in the vertical direction by Pan et al. (2014)), and no temperature or scalar fields were included. Top boundary conditions were zero-flux in the horizontal directions and zero-velocity in the vertical direction ($\partial\tilde{u}_{i,i=1,2}/\partial x_3 = 0, \tilde{u}_3 = 0$ at $x_3 = H$), and the bottom boundary condition was the wall model with $z_0 = 0.001$ m in the horizontal direction and $\tilde{u}_3 = 0$. As in the LES from Pan et al. (2014), canopy height h was set to 2.1 m, and the leaf area density data provided by Wilson et al. (1982) corrected for a small leaf area index difference (rescaled to match the slightly different LAI measured in the field experiment) was used, with a drag coefficient $C_d = 0.25$ and a diagonal projection matrix $P_{11} = P_{22} = 0.25$, $P_{33} = 0.48$. Initial conditions were $\tilde{u}_1 = 10\,\mathrm{m\,s^{-1}}$, $\tilde{u}_2 = \tilde{u}_3 = 0$ in the entire domain, plus the same small fluctuations mentioned in the smooth channel setup. Simulation were evolved for a period of 1 hour, and statistics were obtained by averaging over the last 50 minutes, with additional averaging over 15 realizations to improve statistical convergence. The same ODT parameters from the smooth channel simulations were employed ($C_\lambda = 12.73$ and $Z_\lambda = 0$).

In order to demonstrate the ODT ability in simulating short canopies and the entire ABL at the same time, a second simulation was performed. It corresponded to the ABL with a domain of 1 km, driven by a Coriolis force with $f = 1 \times 10^{-4}\,\mathrm{s^{-1}}$ and capped by a temperature inversion of $3\,\mathrm{K\,km^{-1}}$ above 900 m. The temperature field is included only to create a region of very low turbulence above the ABL, and temperature is set initially as constant (equal to 300 K) below 900 m with zero heat flux at the surface and no heat source or sink within the canopy to keep the neutral stability condition. A total of 5000 grid points were used, creating a simulation with half the resolution inside the canopy compared to the half-channel simulation described above. All the remaining simulation parameters were equal to the half-channel simulation.

In Section 4, ODT results from the two maize canopy simulations are also compared to results from a one-dimensional RANS model with a second-order closure reported by Gleicher et al. (2014) and to the LES results reported by Pan et al. (2014). In all canopy simulation results, u_* is defined as (eddy $\mathrm{flux}^2_{u_1}$ + eddy $\mathrm{flux}^2_{u_2}$)$^{1/4}$ evaluated at canopy top.

3.3. Wind tunnel with waving canopy

The second case used as a reference for ODT with canopy is the wind tunnel experiment presented by Brunet et al. (1994), in which flow statistics within and above a model of waving wheat crop (represented by cylindrical nylon stalks) were measured. The experiment was designed to mimic a neutral surface layer, and a boundary layer of 0.50 ± 0.05 m height with a free-stream velocity of $10.2\,\mathrm{m\,s^{-1}}$ was generated. The canopy had an effective height of 0.047 m, corresponding to stalks of 0.050 m with a natural tendency to bend. The square grid or stalk spacing was 0.005 m, and measurements of vertical profiles of flow statistics were taken at 4.08 m from the leading edge of the canopy (the total canopy length in the streamwise direction was 5.15 m). Profiles of turbulence statistics were calculated over 71 runs, each run with about 17 s of duration.

The ODT simulation designed to mimic this experiment corresponded to a neutral half channel with a domain of 0.55 m, 120 grid points and driven by a constant mean streamwise pressure gradient force $F_1 = 1.5\,\mathrm{m\,s^{-2}}$. Top and bottom boundary conditions and ODT parameters were the same as in the half channel with maize canopy ($C_\lambda = 12.73$, $Z_\lambda = 0$, with $z_0 = 5 \times 10^{-4}$ m). Canopy parameters were set to the values provided by Brunet et al. (1994), namely $h = 0.047$ m, $a = 10\,\mathrm{m^{-1}}$ and $C_d = 0.675$ (note that the drag force is defined with a 1/2 factor by Brunet et al. (1994), which has been incorporated into C_d here), with a diagonal projection matrix $P_{11} = P_{22} = 1$, $P_{33} = 0$. Initial conditions were $\tilde{u}_i = 0$ plus small fluctuations

in the entire domain, and simulation evolved for 600 s. The last 500 s of simulation plus 15 realizations were used for estimation of flow statistics. Two extra simulations with different values of C_λ (C_λ = 6 and 20) are also discussed in Section 4.

3.4. LES of unstable ABL with canopy

The third set of canopy simulations corresponds to the LES setup presented by Patton et al. (2016), where changes in canopy turbulence due to the variation in atmospheric stability from neutral to free convection were investigated. The LES was coupled to a multilayer land surface model representing the hydrological cycle through soil and vegetation, in addition to radiation and photosynthesis models that provide, through an energy budget, vertically resolved sources and sinks of potential temperature θ and water vapor mixing ratio q inside the canopy. The land surface model was implemented as a one-dimensional vertical model inside each grid where canopy was present. Five separate steady-state simulations were performed, one for each atmospheric stability considered (near neutral, weakly unstable, moderately unstable, strongly unstable and free convection).

In order to match the five cases studied by Patton et al. (2016), five ODT simulations with a setup very similar to the LES were performed. As in the LES, all simulations had a vertical domain of 2048 m, with 1024 grid points, driven by a mean pressure gradient which is in geostrophic equilibrium above the ABL ($F_i = f\left(U_g\delta_{i2} - V_g\delta_{i1}\right)$, where $f = 1 \times 10^{-4}\,\mathrm{s^{-1}}$). Top boundary conditions were an imposed horizontal geostrophic wind (U_g, V_g), which varied across simulations (see Table 1) and also corresponded to the initial conditions (set as constant across the entire domain). Other initial conditions were $\tilde{u}_3 = 0$ everywhere, $\tilde{\theta} = 300\,\mathrm{K}$ between the surface and 40 m with an inversion with strength of $3\,\mathrm{K\,km^{-1}}$ above it, and $\tilde{q} = 1\,\mathrm{g\,kg^{-1}}$ everywhere (plus small fluctuations for all variables except $\tilde{q}$). For simplicity, instead of including a coupled land surface model, imposed source profiles $Q_\theta(z)$ and $Q_q(z)$ were used, assumed constant in time and equal to the mean source profiles obtained from the LES and presented in Figure 10 of Patton et al. (2016). In addition, different values of constant heat and water vapor fluxes at the surface were imposed in each simulation (see Table 1). Canopy height was $h = 20\,\mathrm{m}$, $z_0 = 0.001\,\mathrm{m}$ was used in the wall model and a drag coefficient $C_d = 0.15$ with $P_{\alpha\alpha} = 1$ were applied in the drag force. A leaf area density profile representative of a deciduous canopy was used (see Figure 2 of Patton et al. (2016)). Simulations were carried out for 2 hours, and an averaging over the second hour plus fifteen ensembles were performed. All remaining simulation parameters and boundary conditions were the same as in the previous canopy cases.

Even though the ODT model includes non-local fluxes by definition (i.e. as a direct consequence of the mixing across the entire length of the stochastic eddies), it is hard to demonstrate this feature because there is no clear methodology to separate the turbulent flux into local and non-loca components. The approach taken here is to create an extreme, but still relevant, situation in which the non-local flux is clearly dominant. This happens in the presence of fluxes associated with nearly local zero gradients and when the flux is clearly counter-gradient, situations observed in canopy flows when there are more than one concentrated source of passive scalar inside the canopy (Raupach, 1987). We simulate a passive scalar emitted from a bimodal source inside the canopy under near-neutral conditions. This scenario was simulated using an artificial source profile based on the tests by Raupach (1987) with a peak close to canopy top (see Figure 10-a) and a constant surface flux equal to $3 \times 10^{-6}\,\mathrm{g\,kg^{-1}\,m\,s^{-1}}$.

Table 1: Geostrophic wind and surface fluxes of potential temperature and water vapor mixing ratio applied as boundary conditions in the simulations of the Patton et al. (2016) LES canopy case. NN: near neutral, WU: weakly unstable, MU: moderately unstable, SU: strongly unstable, FC: free convection.

	(U_g, V_g) $(\mathrm{m\,s^{-1}})$	$\overline{u_3'\theta'}_0$ $(\mathrm{K\,m\,s^{-1}})$	$\overline{u_3'q'}_0$ $(\mathrm{g\,kg^{-1}\,m\,s^{-1}})$
NN	(20,0)	0.072	1.3×10^{-6}
WU	(10,0)	0.077	1.2×10^{-6}
MU	(5,0)	0.057	6.2×10^{-6}
SU	(2,0)	0.057	4.8×10^{-6}
FC	(0,0)	0.071	1.3×10^{-6}

4. Results and Discussion

4.1. Smooth channel flow

Figure 2 presents vertical profiles of mean flow and turbulence statistics for the ODT simulations of a smooth channel flow with $Re_\tau = 5200$ in "DNS mode" and "LES mode", as well as DNS results for the same flow obtained by Lee and Moser (2015). The choice of the parameters C_λ and Z_λ performed by Schmidt et al. (2003) was based on a match of the ODT mean streamwise velocity profile with DNS results for $Re_\tau = 395$ and 590. Here, similar results for the mean flow between DNS and ODT were obtained using the same parameters, indicating that ODT does not need to be adjusted for different values of Reynolds number. By keeping the same choice of C_λ, ODT in "LES mode" is capable of producing the correct log-law profile, indicating that the choice of the SGS model is appropriate. Furthermore, different from the SGS models proposed by Kerstein and Wunsch (2006), the one used here does not alter the relation between number of stochastic eddies and the available energy (governed by C_λ) of the original flow.

Due to the model's formulation, variances of $\tilde{u}_2$ and $\tilde{u}_3$ are identical in the "DNS mode" case, as the two variables are treated identically (they have the same forcing and boundary conditions, and they are affected equally by the energy redistribution process). A small difference between them is observed in the lowest grid points in the "LES mode" due to the different boundary conditions used (wall model for $\tilde{u}_2$ and zero velocity for $\tilde{u}_3$), but this difference decreases rapidly with increasing distance from the wall. All three velocity variances are underestimated by ODT in the entire domain with respect to DNS results, a problem that seems to be inherent to the ODT model formulation and that has been consistently observed for different types of flows (Kerstein et al., 2001; Schmidt et al., 2003;

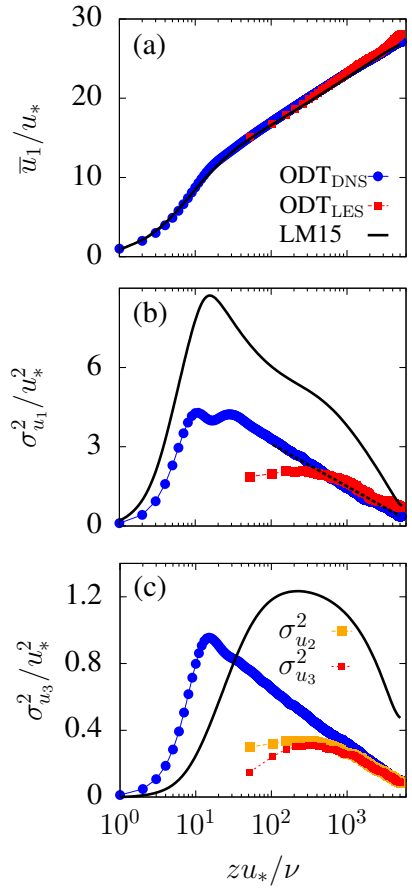

Figure 2: Smooth-channel simulation results: DNS from Lee and Moser (2015) (LM15, black), ODT in "DNS mode" (blue) and in "LES mode" for $dz = 1/200$ (red). (a) Mean streamwise velocity; (b) variance of streamwise velocity; and (c) variance of vertical velocity. In panel (b), the dashed line corresponds to the logarithmic scaling for $\sigma^2_{u_1}$ proposed by Townsend (1976) ($\sigma^2_{u_1}/u^2_* = D_1 + D_2 \ln(z/H)$). Panel (c) also presents the variance of spanwise velocity for ODT in "LES mode" (yellow).

Kerstein and Wunsch, 2006). For ODT in "LES mode", the total variance corresponds only to the "resolved" part (caused by the stochastic model), which are similar to the results from ODT in "DNS mode" in most of the domain except close to the wall, where the size of the eddies eliminated by the use of a much coarser grid impacts the resolved variance.

ODT in "LES mode" with the Smagorinsky-like SGS model produces grid-independent results (Figure 3) without the need of any parameter adjustment, a significant improvement compared to the SGS models proposed by Kerstein and Wunsch (2006). As expected, the SGS model appropriately compensates the lack of momentum flux from stochastic eddies close to the wall when decreasing the model resolution (see Figure 3-c), through the increase in SGS viscosity (Figure 3-d). Variances are similar across different resolutions in most of the domain (Figure 3-b), and the increased contribution from the stochastic model to the resolved variance can be observed close to the wall when resolution is increased. Even though the variance is severely underestimated, the logarithmic scaling for σ^2_u first proposed by Townsend (1976) and observed in the DNS is correctly captured by ODT. When the resolution is decreased to $dz = 1/100$, the resolved variance of streamwise velocity starts to reduce in the entire domain. This is likely because, in this specific example, $dz = 1/100$ already corresponds to a value in which the eddies eliminated by the coarser resolution are relevant in the entire domain, as they are responsible for most of the streamwise velocity variance. Spanwise and vertical velocity variances, on the other hand, are dominated by the energy redistribution process, making the variance similar in most of the domain even for $dz = 1/50$.

4.2. Maize canopy

Canopy flow simulations using ODT are first tested for a maize canopy under neutral atmospheric stability. Figure 4 presents the profiles of flow statistics for the two ODT simulations performed (half channel and full ABL). As observed in the smooth channel case, ODT generates acceptable results (error within 25%) of mean streamwise velocity and momentum flux, combined with significant underestimation (errors between 25 and 50%) of standard deviations of all three velocity components, when compared with field data. Nevertheless, the most interesting aspect of ODT when simulating canopy flows is ODT's ability to represent the vertical transport caused by the mixing-layer eddies originated from shear instability present at canopy top. As the drag force (23) added to (15) produces an inflected profile for streamwise velocity (Figure 4-a), the probability of eddies centered around canopy top with size scaling with h increases significantly. These eddies shuffle properties across a distance that scales with h via the triplet map, producing non-local transport that carries some characteristics of that in real canopy flows.

In the canopy region, non-gaussian velocity statistics are created by sweeps of fast moving air that penetrate the canopy from above, driven by coherent vortical structures present at canopy top (Finnigan, 2000). The sweeps generate positively skewed streamwise velocity statistics, and the vertical asymmetry between the sweeps and ejections due to the loss of kinetic energy to canopy drag results in vertical velocity statistics that are negatively skewed. In addition, the presence of these extreme events results in high kurtosis of both streamwise and vertical velocity. In ODT, the stochastic eddies that scale with canopy height "mix" high-momentum air into the canopy (see Figure 1) resulting in non-gaussian streamwise velocity statistics similar to those observed in the upper canopy and above it (Figures 4-e,f). While the agreement in skewness and kurtosis are fairly good in the upper half of the canopy, in the lower half ODT overestimates the deviations from the Gaussian distribution. This can be understood in the light of the modeling approach adopted here and illustrated in Figure 1. While in the true flow the sweep gradually looses momentum to the canopy, reaching the deep canopy region much weaker than when it enters the canopy, in ODT the reduction is uniform over the entire extension of the eddy, causing the fluctuations in the lower half to be too strong. In addition, the modeling approach in ODT severely impacts the statistics of the vertical velocity fluctuations. Because all the energy in the vertical velocity originates from pressure redistribution (i.e. the second term on the

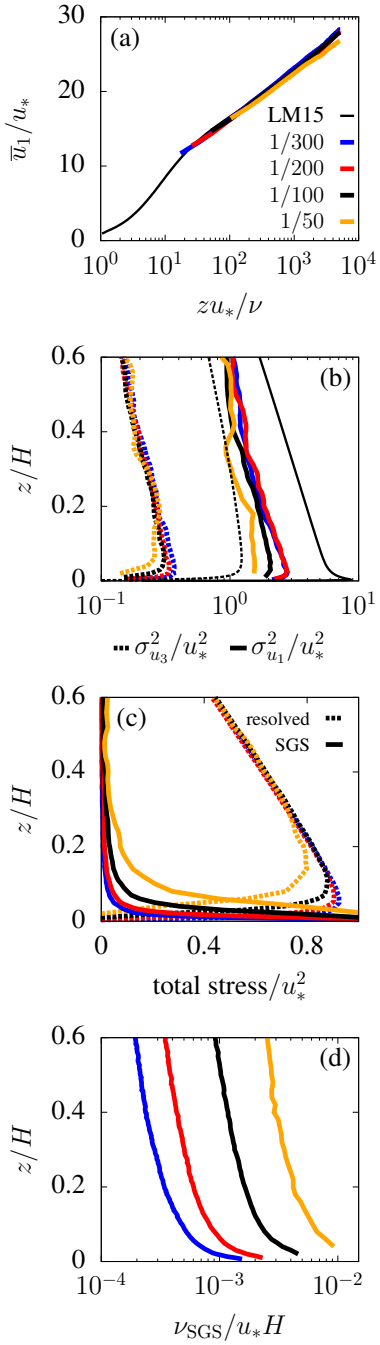

Figure 3: Smooth-channel simulation results: ODT in "LES mode" with dz = 1/300 (blue), 1/200 (red), 1/100 (black) and 1/50 (yellow). (a) Mean streamwise velocity; (b) variance of streamwise velocity (solid lines) and vertical velocity (dashed lines); (c) shear stress from SGS model (solid lines) and from stochastic eddies (dashed lines); and (d) SGS viscosity. In panels (a) and (b) the DNS results from Lee and Moser (2015) are included using thin lines.

right hand side of Equation (3)), ODT cannot capture asymmetries between positive and negative vertical velocity fluctuations (thus having near zero Sk_{u_3}). However, even-order moments such as the kurtosis do not depend on the sign distinction and are captured by the model. The large overestimation of the kurtosis is originated from the same mechanism described above in addition to possible errors originated from the simple treatment of the pressure redistribution.

For a more rigorous test of ODT, probability density functions (PDFs) of normalized streamwise and vertical velocity components from ODT are compared to observations reported by Chamecki (2013) in Figure 5. The agreement between observations and modeled PDFs for streamwise velocity is very good in the upper canopy and reasonable in the lower canopy (where the excessive skewness is clear). With the exception of the lowest level (z/h = 1/3), ODT results are better than reconstructions based on the observed values of skewness and kurtosis obtained from the Gram-Charlier expansion or the Hermitian polinomial transformation presented in Chamecki (2013). For the vertical velocity, the negative side of the PDF is reasonable well predicted, while the positive side is overestimated as a result of the lack of skewness in the vertical velocity produced by ODT.

Profiles of mean flow and turbulence statistics are similar between the simulation of a 1 km-high ABL with a capping inversion and the simulation of the ABL surface layer (simulated as a half-channel flow of 42 m, see Figure 4). An increase in standard deviations and streamwise skewness above the canopy is observed in the ABL case, likely due to the existence of larger eddies. The ABL simulation has a grid spacing that is twice that of the half-channel simulation, requiring a larger contribution from the SGS model. The SGS eddy flux (Figure 4-b) peaks at canopy top as in LES of canopy flows, reaching 18% of the total flux in the ABL case.

Simulations of LES (Pan et al., 2014) and second-order closure RANS (Gleicher et al., 2014) for the same maize canopy are also shown in Figure 4. As expected, LES results show the closer agreement with field data. RANS with a second-order closure provides first- and second-order statistics, and good agreement with observations is obtained. The agreement between ODT results and observations, although not as good as for the two other models, were generated without any case-specific model adjustment (except for the canopy height, drag coefficient and leaf area density, which need to be provided to all models). Furthermore, the ODT simulation of the surface layer took approximately one hour to run all 15 ensembles, whereas the LES with the same domain and half of the vertical resolution from Pan et al. (2014) took approximately one week to run the same simulation time of one ODT ensemble using 24 parallel processors. This approximate comparison helps illustrate where ODT stands in the context of most used canopy modeling tools, with a computational cost that allows the simulation of cases with a larger vertical domain and resolution compared to LES, and with a more general approach in terms of adjustable parameters compared to typical closures of RANS models.

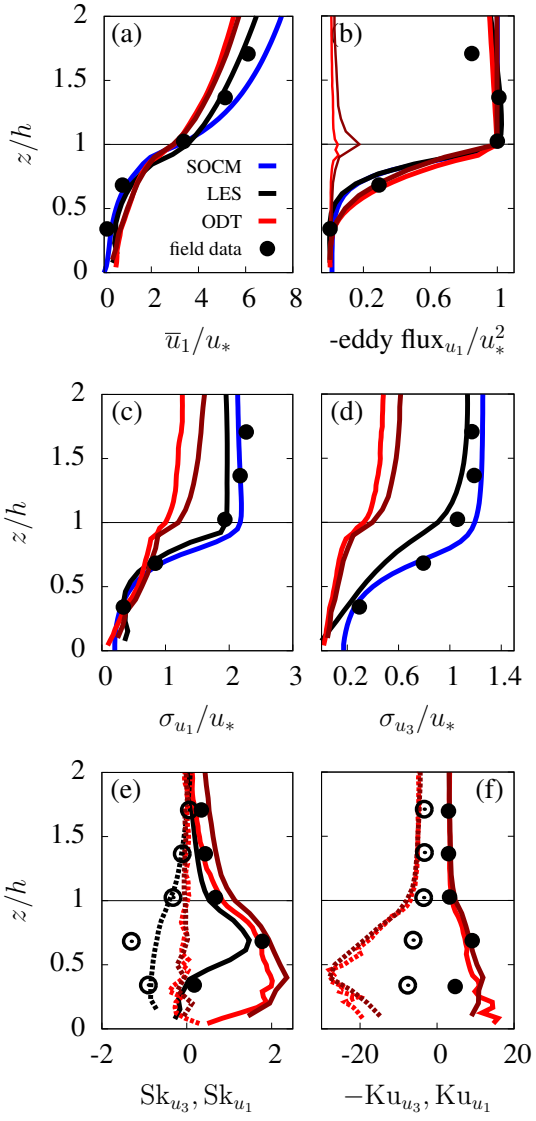

Figure 4: Maize canopy simulation results: field data (circles), RANS with second-order closure model (SOCM) by Gleicher et al. (2014) (blue lines), LES by Pan et al. (2014) (black lines) and ODT results with $H = 42$ m and mean pressure gradient force (red lines) and $z_i = 900$ m and Coriolis force (dark-red lines), where H is the domain size and z_i is the height of the ABL. (a) Mean streamwise velocity; (b) vertical flux of streamwise momentum; (c) standard deviation of streamwise velocity; (d) standard deviation of vertical velocity; (e) skewness of streamwise (solid lines, filled circles) and vertical (dashed lines, open circles) velocity; and (f) kurtosis of streamwise (solid lines, filled circles) and vertical (dashed lines, open circles) velocity. In (b), thin lines correspond to the SGS part of the vertical momentum flux. In all canopy results, u_* is defined as (eddy flux$_{u_1}^2$ + eddy flux$_{u_2}^2$)$^{1/4}$ at canopy top.

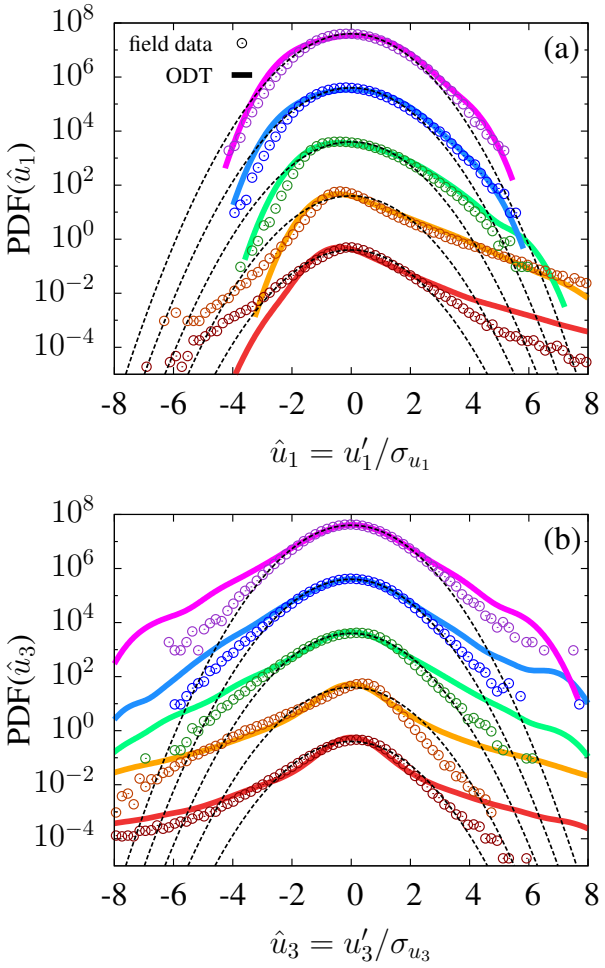

Figure 5: Maize canopy simulation results: field data from Chamecki (2013) (circles) and ODT results (solid lines) of the probability density functions (PDFs) of normalized (a) streamwise and (b) vertical velocity fluctuations $\hat{u}_i = u_i'/\sigma_{u_i}$ (where $u_i' = \tilde{u}_i - \overline{u}_i$) for $z/h = 1/3$ (red), 2/3 (orange), 3/3 (green), 4/3 (blue) and 5/3 (purple), vertically dislocated (from bottom to top).

4.3. Wind tunnel with waving canopy

Overall, the agreement between ODT results and observations for the waving canopy are very similar to those for the maize (Figure 6, red lines): ODT generated reasonable mean profiles of velocity and momentum flux (error lower than 25%), and significantly underestimated (by more than 25%) standard deviations. Skewness and kurtosis measured in the wind tunnel are lower than the ones obtained in the maize field, resulting in a more significant overestimation by ODT in the wind tunnel case. This result indicates that skewness and kurtosis in ODT are highly related to the strength of the streamwise shear (which is similar between wind tunnel and maize canopy cases) whereas in the reality these statistics are results of the complex interaction between turbulent eddies and the canopy.

Figure 6 also presents results from the same simulation using different values for the ODT tunable parameter C_λ. Reducing C_λ reduces the number of eddies and it significantly increases the velocity variances, improving agreement in the second-order moments. However, it compromises the prediction of the mean velocity profile. Increasing C_λ beyond 12.72 causes only very small changes in flow statistics, suggesting that the ODT simulation has already converged to its asymptotic state independent of the number of eddies. Thus, the value of 12.72 is optimal as increasing the value of C_λ increases the number of eddies and the computational cost of the simulation without improving results.

As already mentioned, the underestimation of velocity variances does not imply that turbulent transport is being underestimated. Another test of ODT capabilities in estimating flow statistics using stochastic eddies (despite the low variances) can be seen in the turbulent kinetic energy (TKE) budget terms (Figure 7). The budget for the resolved portion of the TKE in the canopy simulations can be written as

$$P_s + T_t + W_d = \epsilon_{\mathrm{SGS}}. \tag{26}$$

In this equation, which assumes steady-state conditions, P_s is the shear production, T_t is the turbulent transport, W_d is the work done by the resolved velocity field against canopy drag, and ϵ_{SGS} is the SGS dissipation rate (e.g., see Dwyer et al., 1997). In the present ODT simulations, these terms are calculated from

$$P_s = -\text{eddy flux}_{u_i} \frac{\partial \overline{u}_i}{\partial z} \tag{27}$$

$$T_t = -\frac{\partial(\text{eddy flux}_{u_i u_i})}{\partial z} \tag{28}$$

$$W_d = \overline{\tilde{u}_i' d_i'} \tag{29}$$

$$\epsilon_{\mathrm{SGS}} = \overline{\tau_i \partial \tilde{u}_i / \partial z}, \tag{30}$$

where $\tilde{u}_i'$ and d_i' are the fluctuation part of the resolved velocity and drag force, respectively (see Appendix in Kerstein et al. (2001) for a detailed description of the TKE budget in ODT).

All the terms in the TKE budget estimated from ODT are in reasonable agreement with observations, in the sense that the shape of the profiles are similar and the order of magnitude of all quantities are correctly predicted my the model. Small

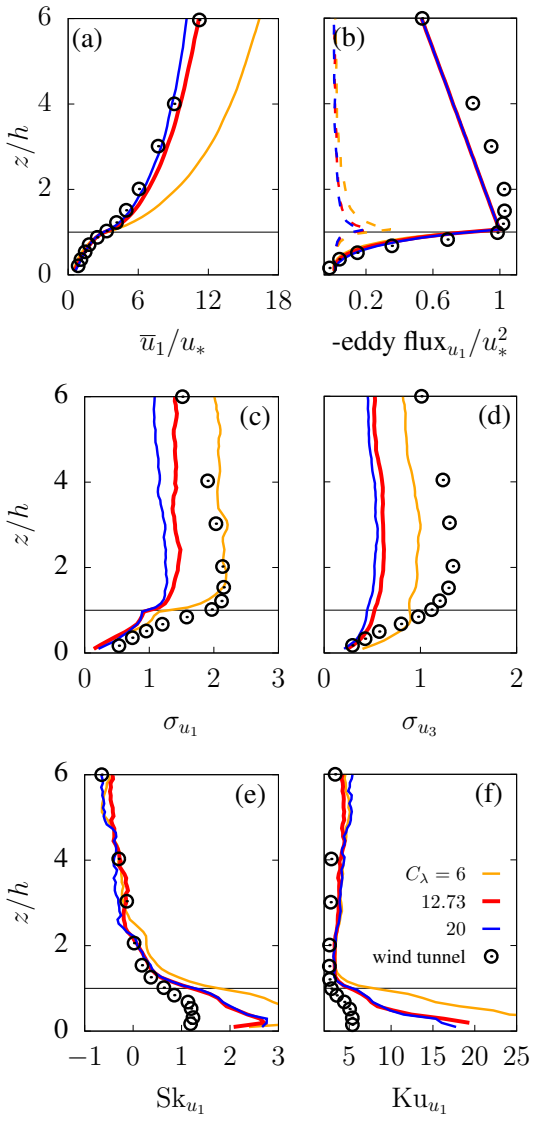

Figure 6: Wind tunnel case: experimental data (circles) and ODT results (solid lines) for $C_\lambda = 6$ (orange), 12.73 (the reference value used for all simulations in red) and 20 (blue). (a) Mean streamwise velocity; (b) vertical flux of streamwise momentum; (c) standard deviation of streamwise velocity; (d) standard deviation of vertical velocity; (e) skewness of streamwise velocity; (f) kurtosis of streamwise velocity. In (b), dashed lines correspond to the SGS part of the vertical momentum flux.

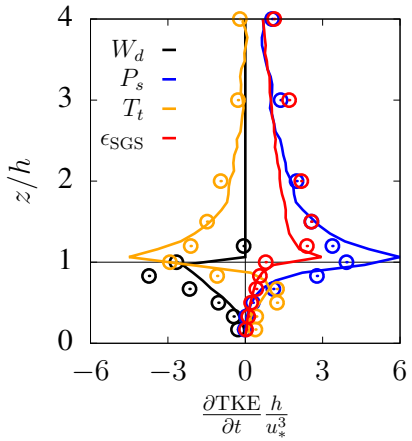

Figure 7: Wind tunnel case, TKE budget terms: work against drag (black); shear production (blue); turbulent transport (yellow); and subgrid scale dissipation rate (red).

discrepancies, such as the position of peaks in production and work against drag, are likely related to the waving nature of the experimental canopy versus the static canopy simulated in ODT (this causes difficulties even in the definition of a canopy height for normalization of the vertical coordinate). The shear production and turbulent transport terms in ODT are defined based on the transport caused by stochastic eddies, rather than vertical velocity fluctuations, which explains the overall agreement despite the severe underestimation of the variances. Due to its inclusion in the energy redistribution term, drag dissipation associated with eddy events is embedded in all terms and cannot be evaluated separately, which may also be a cause for the differences observed between ODT results and wind-tunnel estimations. The work against drag is estimated as a correlation between the velocity fluctuations and the drag force, and its underestimation is likely related to the underestimation of velocity variances. The SGS dissipation is estimated from the SGS model, and it behaves similarly to the energy dissipation from the wind-tunnel data especially inside the canopy, a promising result given that profiles of TKE dissipation rate are needed in several applications, such as Lagrangian Dispersion Models (Poggi et al., 2006), and are particularly difficult to estimate from measurements. The overall qualitative agreement between ODT and wind-tunnel observations suggests that even the complex TKE budget within and above the canopy is reasonable well reproduced by ODT.

4.4. LES with canopy by Patton et al. (2016)

The impact of unstable atmospheric conditions in canopy flows was investigated using LES for the first time by Patton et al. (2016), and it is reproduced here using ODT. This is a challenge for LES because it requires the model domain to represent the entire depth of the ABL with fine enough resolution to represent in-canopy processes. Profiles of mean flow and turbulence statistics for five different stabilities, ranging from near neutral to free convection, are shown in Figure 8. Under near-neutral conditions, ODT has a performance comparable to the previous canopies: reasonable agreement for mean streamwise velocity and vertical momentum flux, underestimation of velocity standard deviations. The overestimation of streamwise velocity skewness is more accentuated than in the maize case, as this deciduous-like canopy presents a lower skewness with a peak higher in the canopy compared with the maize, whereas ODT results are similar for both canopies.

LES results showed that increasing thermal instability (obtained mainly through a reduction in the imposed geostrophic wind), resulted in a reduction in normalized mean streamwise velocity, momentum flux and skewness, combined with a decrease in normalized velocity standard deviations between near neutral, weakly unstable and moderately unstable conditions and a less significant decrease between moderately unstable, strongly unstable and free convection. ODT simulations were able to capture this patterns, reaching values of vertical velocity standard deviations that are closer to LES results (error smaller than 25%) under more unstable conditions. This result suggests that, for ABL conditions, ODT has more difficulty in reproducing shear-driven variance than buoyancy-driven variance.

Despite the poor agreement in vertical velocity variance, mean vertical turbulent transport can still be successfully represented by ODT. An example of this situation is shown in Figure 9, where the profiles of mean concentration, vertical flux and standard deviation of an active scalar (potential temperature) and a passive scalar (water vapor mixing ratio) are presented. As expected, vertical fluxes show good agreement as they are a direct consequence of the source terms imposed in the simulation. The mean profiles also show reasonable agreement with LES results for all stabilities considered. Standard deviations are around the correct values, with some discrepancies in the shape of the profiles. For example, in the lower half of the canopy for the more unstable cases, LES generated lower values of potential temperature standard deviation than ODT. The values of σ_q/q_* presented a peak closer to the canopy top and lower values at canopy bottom in LES than in ODT. In spite of that, overall the transport of scalars inside and immediately above the canopy is well reproduced by ODT in all the range of stabilities between neutral and free convection, without any model adjustment or specific closure, only by defining the appropriate forcing, sources and boundary conditions.

Finally, results for the simulation with a bimodal scalar source designed to test non-local fluxes are shown in Figure 10. The presence of two strong localized sources produces a mean concentration profile with large variations on vertical distances comparable to the extent of shear layer eddies. The vertical fluxes produced by ODT show both counter-gradient and nearly zero-gradient flux regions (see blue and red regions in Figure 10). The counter-gradient flux is the result of large eddies that carry low concentrations from above the canopy deep into the vegetation, overwhelming the local negative flux produced by the localized peak in concentration. This result can be compared to Figure 9 in Raupach (1987), which shows a qualitatively similar result using a Lagrangian approach for homogeneous turbulence. We conclude that ODT is capable of qualitatively reproducing one of the most challenging aspects of canopy turbulence, the non-local transport by shear layer ed-

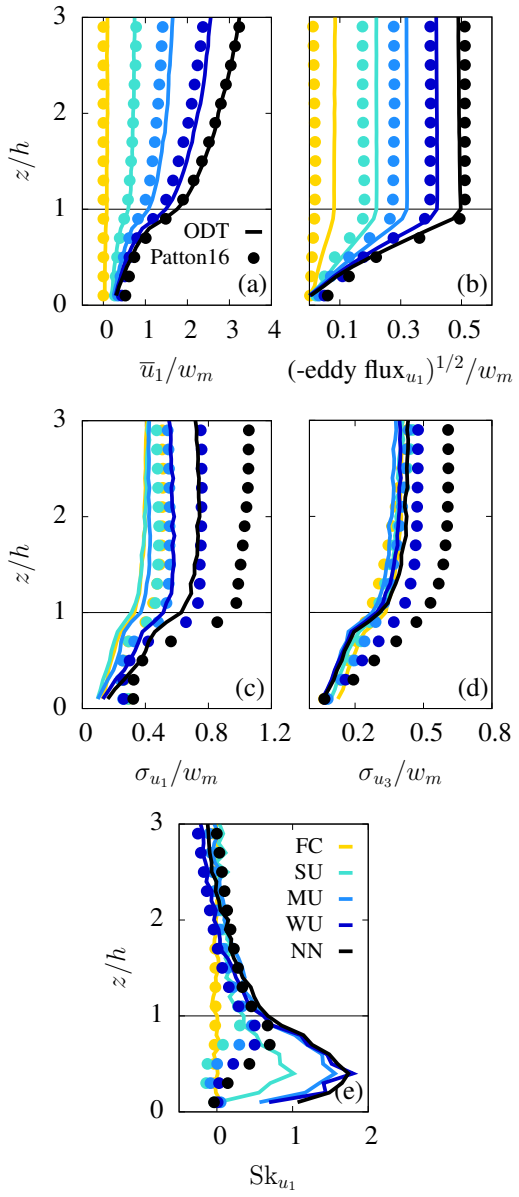

Figure 8: Results from simulations of Patton et al. (2016): LES by Patton et al. (2016) (circles) and ODT (solid lines) results for near-neutral (NN, black), weakly unstable (dark-blue), moderately unstable (MU, blue), strongly unstable (SU, turquoise) and free-convection (FC, yellow) conditions. (a) Mean streamwise velocity; (b) square root of the vertical flux of streamwise momentum; (c) standard deviation of streamwise velocity; (d) standard deviation of vertical velocity; and (e) skewness of streamwise velocity. All variables except for skewness are normalized by $w_m = (w_*^3 + 5u_*^3)^{1/3}$, where $w_* = (g\overline{u_3'\theta'}_0 z_i/\theta_*)^{1/3}$.

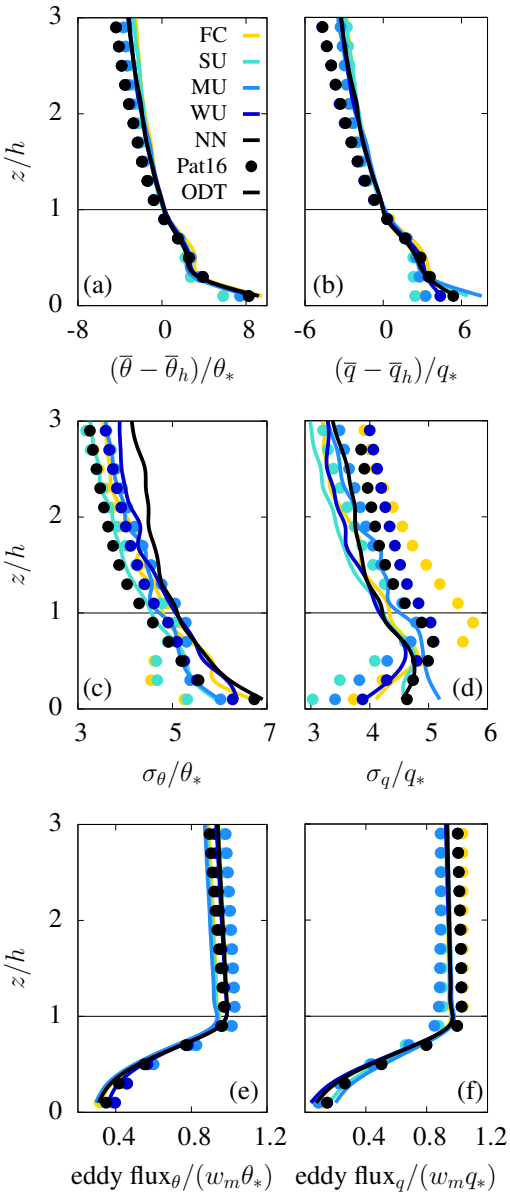

Figure 9: Results from simulations of Patton et al. (2016) (as in Figure 8): Mean profile of (a) potential temperature and (b) water vapor mixing ratio; standard deviation of (c) potential temperature and (d) water vapor mixing ratio; vertical flux of (e) potential temperature and (f) water vapor mixing ratio. The normalizing variables are defined as $\theta_* = \left(\int_0^h Q_\theta dz + \overline{\tilde{u}_3'\tilde{\theta}'}_0\right) w_m^{-1}$ and $q_* = \left(\int_0^h Q_q dz + \overline{\tilde{u}_3'\tilde{q}'}_0\right) w_m^{-1}$.

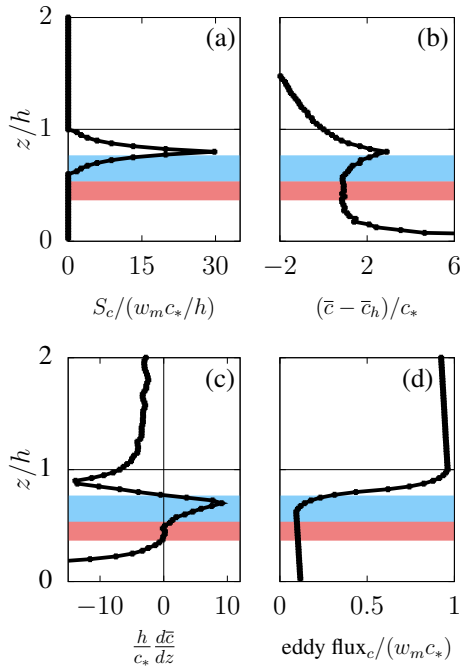

Figure 10: Result from the near-neutral simulation of Patton et al. (2016) for a bimodal scalar source: (a) source profile; (b) mean concentration profile; (c) mean vertical gradient; and (d) vertical turbulent flux of a passive scalar. Normalizing variables are defined as in Figures 8 and 9. Blue and red shaded areas indicate the regions of counter-gradient and nearly-zero gradient fluxes, respectively.

dies in the near-field of localized sources (Chamecki, 2013).

4.5. Summary of ODT performance in canopy flows

For the types of canopies tested here, most of the mean streamwise velocity generated by ODT was within 25% from the reference values (direct measurements or LES), and no clear tendency of under or over estimation was observed (Figure 11-a). Similarly, the vertical momentum flux was mostly around or below 25% error (Figure 11-b), except for significant errors (more than 50%) when flux values were very low (close to the ground and under free convection for the LES with deciduous case). The ODT tendency of underestimating velocity standard deviation can be clearly seen in Figures 11-c,d, which shows that ODT errors reached values up to ~50% in most of cases and canopy regions, and the error was higher than 50% in the region closer to the ground for the streamwise direction. The vertical velocity standard deviation presented significant underestimation (error higher than 50%) in the maize case in the upper canopy and above canopy regions, and presented a systematic error reduction with increasing instability in the case of LES with deciduous canopy. The overestimation of streamwise skewness (Figure 11-e) was of more than 50% in the lower canopy and in some regions of upper canopy (especially in the LES with deciduous case, in which peaks in skewness were lower in the canopy in ODT compared to LES). Overall, the ODT performance is consistent across different canopies, and the only clear variation on the error observed here is the impact of atmospheric stability on σ_{u_3}. However, as in the skewness of streamwise velocity case (which was close to reference values in the maize case but not in the other two canopies), the good performance of σ_{u_3} in ODT under high instability may be different for other canopies, so more tests are needed in order to provide a conclusion on this matter.

5. Conclusions

In this work, Kertein's One-Dimensional Turbulence (ODT) model was modified and used to perform simulations of canopy flows. In order to preserve the low computational cost that makes ODT advantageous for ABL simulations, a filtered version of the ODT model was developed. In this approach, only the large scales of turbulence are represented by stochastic eddies, and an eddy-viscosity SGS model is used to represent the effects of unresolved turbulence. In addition, the energetics of the stochastic eddies that penetrate the canopy were modified to account for the fact that these eddies loose energy by performing work against the drag force imposed by the canopy elements.

Model results are consistent with previous performances of ODT without the SGS model and canopy: reasonable mean field profiles and vertical fluxes of momentum and scalars and underestimated profiles of variances. All results presented here were obtained with values of the ODT adjustable parameter C_λ and canopy drag coefficients defined in previous studies, i.e., no case-specific adjustment was performed here. Different ways of representing SGS turbulence have been tested and could be proposed, but the fact that the simple approach proposed here maintains ODT performance for several grid resolutions without the need of parameter adjustments indicates that the Smagorinsky-like model is a suitable approach.

Despite its one-dimensional nature, ODT is deemed capable of reproducing a number of non-trivial features of canopy flows that originate in the complex interaction between the turbulent field and the vegetation. Some of these features are quantitatively accurate and others are qualitatively correct but over/underpredicted. The combination of reasonable predictions of mean velocity and momentum flux profiles (as well as mean profiles for scalars and their corresponding vertical fluxes) indicates that ODT is capable of representing the non-local fluxes that dominate the dynamics of canopy flows and that impose severe limitations in the use of eddy-viscosity and eddy-diffusivity approaches. This is a direct consequence of the stochastic eddy formulation of the model, which appropriately converts the direct effect of body forces acting on the flow into turbulent transport through the probability distribution of non-local eddies. The strongly non-Gaussian PDFs of streamwise velocity fluctuations is fairly well predicted by ODT. To put this result in perspective, note that even models that predict the PDF from observed values of skewness and kurtosis based on the Gram-Charlier expansion or on Hermite polynomial transformations have difficulties (Chamecki, 2013). ODT also does a reasonable job in reproducing vertical profiles of the TKE budget terms (including the TKE dissipation rate) and the main effects of buoyancy on canopy flows. Although in these

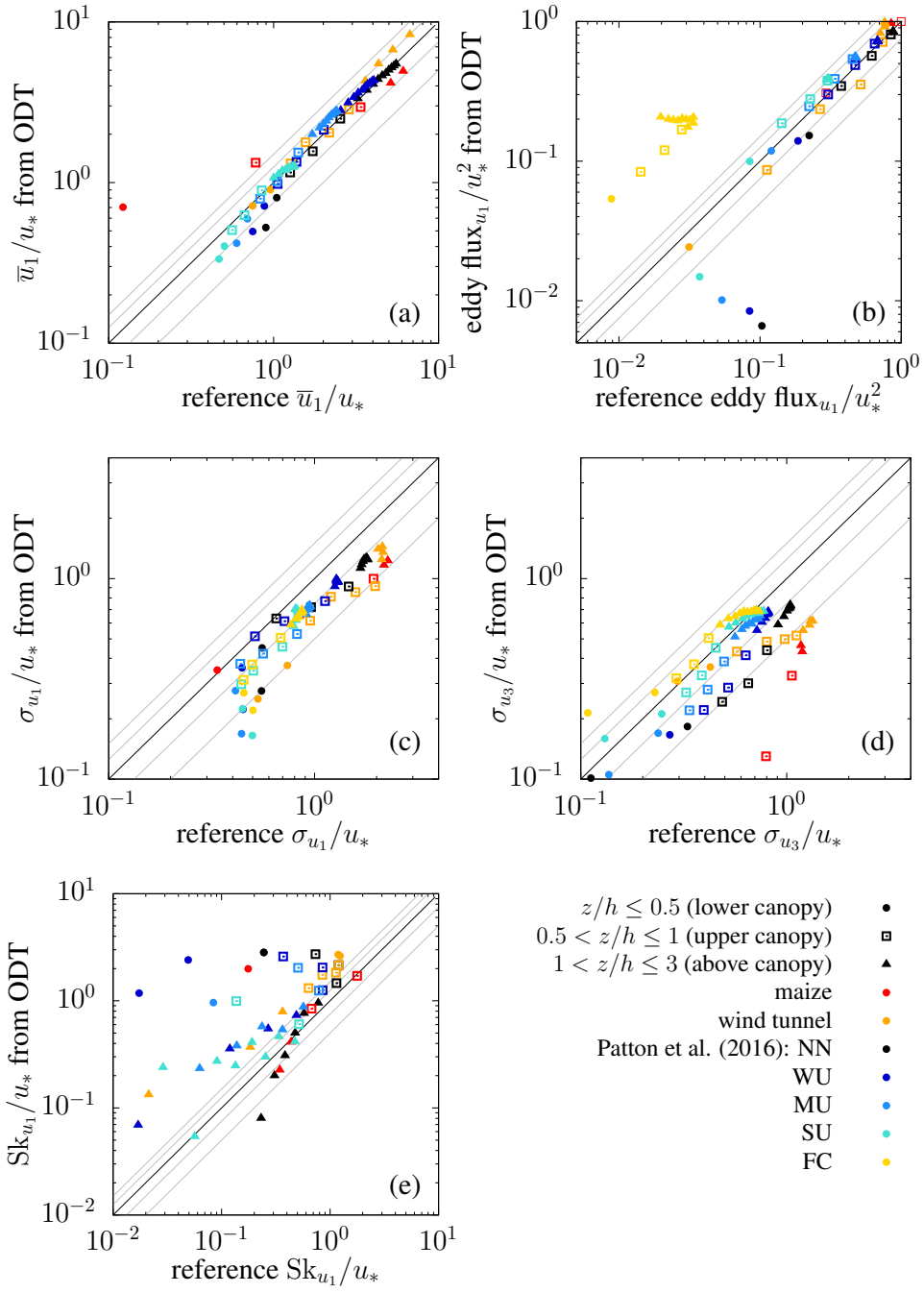

Figure 11: ODT versus reference values (observational data from maize and wind tunnel or LES from (Patton et al., 2016)) of (a) streamwise velocity; (b) vertical momentum flux; standard deviation of (c) streamwise and (d) vertical velocity; and (e) streamwise skewness. Data are separated into lower canopy ($z/h \leq 0.5$, circles), upper canopy ($0.5 < z/h \leq 1$, squares) and above canopy ($1 < z/h \leq 3$, triangles). Maize canopy (red), wind tunnel with waving canopy (orange), LES with canopy by Patton et al. (2016) for near-neutral (black), weakly unstable (dark-blue), moderately unstable (MU, blue), strongly unstable (SU, turquoise) and free-convection (FC, yellow) conditions. Black line corresponds to the 1:1 reference line, gray lines correspond to ± 25% and 50%. Results for the Patton et al. (2016) case are normalized by $5^{-1/3}w_m$ (which corresponds to u_* in the near-neutral case).

cases the agreement is less satisfactory from a quantitative perspective, they are good examples of an important characteristic of ODT: the ability in representing non-trivial flow features through a general phenomenological approach.

In order to improve ODT performance in simulating canopy flows, it would be desirable to fix the issues related to the underestimation of total TKE and the lack of asymmetry in the vertical velocity distributions (characterized by the negligible odd-order moments). The TKE produced in the flow is a direct consequence of how the triplet map (Equation 5) acts in converting mean shear into TKE. In principle, the triplet map could be replaced by another formulation, although at this point there is no evidence that this approach would necessarily improve the total TKE. The triplet map is a good choice because it creates a uniform strain rate and length-scale reduction, in addition to having the smallest possible eddy size (equal to 6 dz) when compared to other mapping functions (such as the "quintuplet map" tested by Kerstein (1991) in a precursor of the ODT model). In ODT, all the energy in the vertical velocity originates from the model for pressure redistribution. In its current formulation, this approach renders the vertical velocity predictions incapable of asymmetries between positive and negative fluctuations (i.e. zero odd-order moments) despite the fact that the fat tails in the PDF of vertical velocity are present (although severely over predicted). This is problematic in canopy flows and, likely, also in simulations of convective ABLs. It is possible that different energy redistribution formulations that take into account differences in vertical velocity fluctuations generated by buoyancy and canopy drag, for example, would significantly improve model performance.

The use of ODT to simulate stable ABL has been previously shown to be feasible (Kerstein and Wunsch, 2006), and although it has not been tested here, there is no specific reason to expect a different outcome in the simulation of stable flows with canopy. The model may not be appropriate, however, to represent flows with very low or intermittent turbulence condition, which can be also the case of very dense and tall forests where the turbulence inside the canopy is extremely low.

Finally, we note that ODT can also be used to simulate transient conditions or a two-dimensional steady-state flow (by converting the time dimension into streamwise direction through a bulk streamwise velocity), and these capabilities still need to be explored in the context of canopy flows. In addition, ODT can be coupled to large scale models instead of being used as a stand-alone single column model. ODT has been used as a wall-model for LES of high-Reynolds number turbulence in channel flow (Schmidt et al., 2003). In the context of LES of ABL flows, one can certainly envision ODT as a wall model used to resolve complex physical phenomena close to the ground that cannot be resolved in the numerical grid. As an example, one could use ODT to resolve a crop canopy that cannot be resolved in the LES grid of an ABL simulation. In the same line of reasoning, one could envision the use of ODT as an alternative to the traditional surface exchange parameterizations or canopy/urban submodels used in regional models such as the Weather Research and Forecasting (WRF) model or even in climate models.

Acknowledgments

LFS was funded by CNPq/Brazil through the program Science Without Borders. MC was supported by National Science Foundation Grant AGS1358593. We thank Alan R. Kerstein for insightful discussions and for making the ODT basic codes available (at https://sites.google.com/site/odtresearch/codes), and four anonymous reviewers for comments that greatly improved the manuscript.

Albertson, J.D., Katul, G.G., Wiberg, P., 2001. Relative importance of local and regional controls on coupled water, carbon, and energy fluxes. Advances in Water Resources 24, 1103 1118.

Brunet, Y., Finnigan, J., Raupach, M., 1994. A wind tunnel study of air flow in waving wheat: Single-point velocity statistics. Boundary-Layer Meteorology 70, 95–132.

Bryan, A.M., Bertman, S.B., Carroll, M.A., Dusanter, S., Edwards, G.D., Forkel, R., Griffith, S., Guenther, A.B., Hansen, R.F., Helmig, D., Jobson, B.T., Keutsch, F.N., Lefer, B.L., Pressley, S.N., Shepson, P.B., Stevens, P.S., Steiner, A.L., 2012. In-canopy gas-phase chemistry during cabinex 2009: sensitivity of a 1-d canopy model to vertical mixing and isoprene chemistry. Atmospheric Chemistry and Physics 12, 8829–8849.

Cassiani, M., Radicchi, A., Albertson, J., 2007. Modelling of concentration fluctuations in canopy turbulence. Boundary-Layer Meteorology 122, 655–681.

Chamecki, M., 2013. Persistence of velocity fluctuations in non-gaussian turbulence within and above plant canopies. Physics of Fluids 25, 1–14.

Deardorff, J.W., 1970. A numerical study of three-dimensional turbulent channel flow at large reynolds numbers. Journal of Fluid Mechanics 41, 453–480.

Dwyer, M.J., Patton, E.G., Shaw, R.H., 1997. Turbulent kinetic energy budgets from a large-eddy simulation of airflow above and within a forest canopy. Boundary-Layer Meteorology 84, 23–43.

Finnigan, J., 2000. Turbulence in plant canopies. Annual Review of Fluid Mechanics 32, 519–571.

Germano, M., Piomelli, U., Moin, P., Cabot, W.H., 1991. A dynamic subgrid-scale eddy viscosity model. Physics of Fluids A 3, 1760–1765.

Gleicher, S.C., Chamecki, M., Isard, S.A., Pan, Y., Katul, G.G., 2014. Interpreting three-dimensional spore concentration measurements and escape fraction in a crop canopy using a coupled eulerian-lagrangian stochastic model. Agricultural and Forest Meteorology 194, 118–131.

Harman, I.N., Finnigan, J.J., 2007. A simple unified theory for flow in the canopy and roughness sublayer. Boundary-Layer Meteorology 123, 339–363.

Harman, I.N., Finnigan, J.J., 2008. Scalar concentration profiles in the canopy and roughness sublayer. Boundary-Layer Meteorology 129, 323–351.

Huang, J., Katul, G., Albertson, J., 2013. The role of coherent turbulent structures in explaining scalar dissimilarity within the canopy sublayer. Environmental Fluid Mechanics 13, 571–599.

Juang, J.Y., Katul, G.G., Siqueira, M.B., Stoy, P.C., McCarthy, H.R., 2008. Investigating a hierarchy of eulerian closure models for scalar transfer inside forested canopies. Boundary-Layer Meteorology 128, 1–32.

Katul, G., Albertson, J., 1998. An investigation of higher-order closure models for a forested canopy. Boundary-Layer Meteorology 89, 47–74.

Katul, G., Grönholm, T., Launiainen, S., Vesala, T., 2011. The effects of the canopy medium on dry deposition velocities of aerosol particles in the canopy sub-layer above forested ecosystems. Atmospheric Environment 45, 1203–1212.

Kerstein, A., Ashurst, W.T., Wunsch, S., Nilsen, V., 2001. One-dimensional turbulence: vector formulation and application to free shear flows. Journal of Fluid Mechanics 447, 85–109.

Kerstein, A.R., 1991. Linear-eddy modelling of turbulent transport. part 6. microstructure of diffusive scalar mixing fields. Journal of Fluid Mechanics 231, 361–394.

Kerstein, A.R., 1999. One-dimensional turbulence: model formulation and application to homogeneous turbulence, shear flows, and buoyant stratified flows. Journal of Fluid Mechanics 392, 277–334.

Kerstein, A.R., Wunsch, S., 2006. Simulation of a stably stratified atmospheric boundary layer using one-dimensional turbulence. Boundary-Layer Meteorology 118, 325–356.

Kumar, V., Kleissl, J., Meneveau, C., Parlange, M.B., 2006. Large-eddy simulation of a diurnal cycle of the atmospheric boundary layer: Atmospheric stability and scaling issues. Water Resources Research 42, W06D09.

Lee, M., Moser, R.D., 2015. Direct numerical simulation of turbulent channel flow up to $Re_\tau \approx 5200$. Journal of Fluid Mechanics 774, 395–415.

Lilly, D.K., 1967. The representation of small-scale turbulence in numerical simulation experiments, in: Proc. IBM Scientific Computing Symposium on Environmental Sciences, p. 195.

Mason, P.J., Thomson, D.J., 1992. Stochastic backscatter in large-eddy simulations of boundary layers. Journal of Fluid Mechanics 242, 51–78.

Massman, W., Weil, J., 1999. An analytical one-dimensional second-order closure model of turbulence statistics and the lagrangian time scale within and above plant canopies of arbitrary structure. Boundary-Layer Meteorology 91, 81–107.

Pan, Y., Chamecki, M., Isard, S.A., 2014. Large-eddy simulation of turbulence and particle dispersion inside the canopy roughness sublayer. Journal of Fluid Mechanics 753, 499–534.

Patton, E.G., Sullivan, P.P., Shaw, R.H., Finnigan, J.J., Weil, J.C., 2016. Atmospheric stability influences on coupled boundary layer and canopy turbulence. Journal of the Atmospheric Sciences 73, 1621–1647.

Piomelli, U., Moin, P., Ferziger, J.H., 1988. Model consistency in large eddy simulation of turbulent channel flows. The Physics of Fluids 31, 1884–1891.

Poggi, D., Katul, G., Albertson, J., 2006. Scalar dispersion within a model canopy: Measurements and three-dimensional lagrangian models. Advances in Water Resources 29, 326–335. Experimental Hydrology: A Bright Future.

Porté-Agel, F., Meneveau, C., Parlange, M.B., 2000. A scale-dependent dynamic model for large-eddy simulation: application to a neutral atmospheric boundary layer. Journal of Fluid Mechanics 415, 261–284.

Raupach, M.R., 1987. A lagrangian analysis of scalar transfer in vegetation canopies. Quarterly Journal of the Royal Meteorological Society 113, 107–120.

Reynolds, A.M., 1998. On the formulation of lagrangian stochastic models of scalar dispersion within plant canopies. Boundary-Layer Meteorology 86, 333–344.

Schmidt, J.R., Wendt, J.O., Kerstein, A.R., 2009. Non-equilibrium wall deposition of inertial particles in turbulent flow. Journal of Statistical Physics 137, 233–257.

Schmidt, R.C., Kerstein, A.R., Wunsch, S., Nilsen, V., 2003. Near-wall LES closure based on one-dimensional turbulence modeling. Journal of Computational Physics 186, 317–355.

Shaw, R.H., Patton, E.G., 2003. Canopy element influences on resolved- and subgrid-scale energy within a large-eddy simulation. Agricultural and Forest Meteorology 115, 5 – 17. A tribute to George W. Thurtell's contributions in micrometeorology.

Shaw, R.H., Schumann, U., 1992. Large-eddy simulation of turbulent flow above and within a forest. Boundary-Layer Meteorology 61, 47–64.

Smagorinsky, J., 1963. General circulation experiments with the primitive equations i. the basic experiment. Monthly Weather Review 91, 99–164.

Su, H.B., Shaw, R., Paw, K., Moeng, C.H., Sullivan, P., 1998. Turbulent statistics of neutrally stratified flow within and above a sparse forest from large-eddy simulation and field observations. Boundary-Layer Meteorology 88, 363–397.

Thomson, D.J., 1987. Criteria for the selection of stochastic models of particle trajectories in turbulent flows. Journal of Fluid Mechanics 180, 529–556.

Townsend, A., 1976. The structure of turbulent shear flow.

Wilson, J.D., Sawford, B.L., 1996. Review of lagrangian stochastic models for trajectories in the turbulent atmosphere. Boundary-Layer Meteorology 78, 191–210.

Wilson, J.D., Ward, D.P., Thurtell, G.W., Kidd, G.E., 1982. Statistics of atmospheric turbulence within and above a corn canopy. Boundary-Layer Meteorology 24, 495–519.

Wilson, N.R., Shaw, R.H., 1977. A higher order closure model for canopy flow. Journal of Applied Meteorology 16, 1197–1205.

Yamazaki, T., Kondo, J., Watanabe, T., Sato, T., 1992. A heat-balance model with a canopy of one or two layers and its application to field experiments. Journal of Applied Meteorology 31, 86–103.